Materials Research Express

Samarium and yttrium doping induced phase transitions and their effects on the structural, optical and electrical properties of Nd2Sn2O7 ceramics

To cite this article before publication: Adli Saleh *et al* 2020 *Mater. Res. Express* in press https://doi.org/10.1088/2053-1591/ab67f7

Samarium and yttrium doping induced phase transitions and their effects on the structural, optical and electrical properties of $Nd_2Sn_2O_7$ ceramics

Adli A. Saleh[1], A. F. Qasrawi [1,3,*], Hanan Z. Hamamera[1], Hazem K. Khanfar [2], G. Yumusak[4]
[1]*Department of Physics, Arab American University, Jenin, Palestine*
[2]*Department of Telecommunication Engineering, Arab American University, Jenin, Palestine*
[3]*Faculty of Engineering, Atilim University, 06836 Ankara, Turkey*
[4]*Metallurgical and Materials Engineering Dept., Marmara University, 34722 Istanbul, Turkey*
E-mail: atef.qasrawi@atilim.edu.tr , atef.qasrawi@aaup.edu

Abstract

In this work, the effects of Sm^{+3} and Y^{+3} doping onto the structural, optical and electrical properties of $Nd_2Sn_2O_7$ are investigated. An atomic content of 3.49 % and 4.29% of Sm and Y, respectively, were sufficient to alter the physical properties of the $Nd_2Sn_2O_7$. Particularly, the Y^{+3} ionic substitution decreased the lattice constant, narrows the energy band gap, changed the conductivity type from $n-$to p- type and increased the electrical conductivity by 73 times without changing the cubic nature of structure of the pyrochlore ceramics. On the other hand, Sm^{+3} ionic substitutions changed the cubic structure to hexagonal or trigonal and forced optical transitions in the infrared range of light. The energy band gap shrunk from 3.40 to 1.40 eV, the defect density is reduced and the electrical conductivity increased by 47 times via Sm doping. These doping agents' makes the neodymium stannate pyrochlore ceramics more appropriates for optoelectronic applications.

Keywords: Neodymium stannate; Rare earth doping; lattice parameters; band gap; conductivity

* Author to whom any correspondence should be addressed.

1. Introduction

Pyrochlore ceramics including neodymium stannate are regarded as promising materials owing to their suitability for use as nanofibers and efficient photoabsorbers [1], as photocatalytic agents [2], as magnetocaloric applications [3] and as optoelectronic devices [4, 5, 6]. Nanofibers and thin films made of $Nd_2Sn_2O_7$ and other rare earth materials like $Sm_2Sn_2O_7$ and $Er_2Sn_2O_7$ which are prepared by the electrospinning and spin coating techniques [1] are reported to exhibit high photoelectrochemical

efficiency for water splitting reactions. Nanostructured $Nd_2Sn_2O_7$ are also used for degradation methyl orange dye [2]. $Nd_2Sn_2O_7$ is also observed to exhibit a second order magnetic phase transition at 0.91 K to a noncoplanar all-in-all-out magnetic structure of the Nd^{3+} magnetic moments making the material suitable for magnetocaloric applications [3]. In addition, optical investigations on the neodymium stannate pyrochlore ceramics have shown that with the energy band gap being 3.40 eV, the pyrochlore are attractive for the production of ultraviolet sensors [4].

In an attempt to widen the range of applications of the $Nd_2Sn_2O_7$ pyrochlore ceramics, various doping agents including Mn [7], Gd and Tb metals are used [8]. While, the participation Mn significantly influenced the textural properties, the bond strength of Sn–O, surface oxygen vacancy and redox properties of the $Nd_2Sn_2O_7$ pyrochlore ceramics as catalysts [7, 9, 10], the Gd and Tb doping narrowed the energy band gap and altered the conductivity type of the pyrochlore by forming either shallow acceptor or deep donor levels in the band gap of the pyrochlore. The doping agents presented by Gd and Tb remarkably enhanced the electrical conductivity 390 and 58 times, respectively. The studies suggests that the neodymium stannate are highly influenced by the doping agents which plays role in technological applications. Although the Tb and Gd doping succeed in altering the conduction type and energy band gap values, they did not succeed in reaching the low energy spectral ranges. Solar cell and infrared applications require low energy band gap values. For this reason, here in this work, we are motivated to explore the effects of the other rare earth samarium and yttrium doping agents on the structural, optical and electrical properties of the pyrochlore. These two elements are selected because of their electronic properties. Namely, the yttrium exhibit electronic configuration in the orbital states $\boldsymbol{4d^1 5s^2}$ which is close to the orbitals of Sn ($\boldsymbol{4d^{10} 5s^2 5p^2}$) and samarium have electronic configuration with the orbital states $\boldsymbol{4f^6 6s^2}$ which is close to those of Nd ($\boldsymbol{4f^4 6s^2}$). The close orbitals forces orbital overlapping that in turn enhances the electronic properties of the pyrochlore ceramics. We believe that

slight enrichment in the doping level (2% for Gd and Tb is enriched to 4.0% for Sm and Y) and altering the number of electrons in the same orbital states may change the dynamics of the optical transitions and make the material more appropriate for solar energy harvesting and IR other IR applications.

Here in this work, low percentages of Sm and Y are solved in the structure of the pyrochlore by the solid state reaction technique. The resulting pyrochlore are studied by means of scanning electron microscopy, X-ray diffraction and optical spectrophotometry to determine the effects of the doping agents on the crystallinity, grain and crystallite size, microstrain, defect density, optical absorption interbands transitions and bang gap values. In addition, the temperature dependent electrical conductivity is also studied to determine the effects of the doping agents on the electrical conductivity parameters prior to technological applications.

2. Experimental Details

Sm and Y- doped $Nd_2Sn_2O_7$ pyrochlore ceramics are synthesized by the conventional solid state reaction technique using appropriate high purity (99.9% pure) Nd_2O_3, SnO_2, Sm_2O_3 or Yb_2O_3 starting materials. The value of the empirical doping level was chosen to be 4.0% of Sm_2O_3 or Y_2O_3. The oxides were weighed (using a 5- significant digit scale) and mixed in accordance with the empirical formula $Nd_{2-x}(Sm_x, or\ Y_x)Sn_2O_7$. The mixing was actualized in ethanol media in a plastic container for 6 h. After drying the slurries at 100 °C for 24h, they were calcined at 1050-1400 °C for 10h in a tightly closed alumina crucible to prevent evaporation losses which were checked by weighing the samples before and after calcination. After grinding the calcined powders in an agate mortar, they were pressed into pellets with 10 mm diameters and 1–2 mm thickness using uniaxial press with 2MPa pressure. The pellets were sintered in the temperature range of 1050-1400 °C for 4h with a heating and cooling rates of 250 °C/h

after burying them in the pyrochlore powder to minimize the loss of volatile species. Bulk densities of the samples were measured by Archimedes method after grinding the surfaces of the pellets to maintain proper density measurements. The relative densities of the pellets were calculated using theoretical densities of the doped BZN samples which were estimated using the respective lattice parameters of each sample that are obtained from X-ray diffraction. The best calcination and sintering temperatures were the same (1350 ^{o}C) for revealing optimum parameters to reveal highest possible relative density (~98%). The samarium doped samples were wheat (one of the brown tones) colored and the Y-doped samples were ivory colored. The ceramics were investigated by scanning electron microscopes (COXEM- 200 equipped with EDAX energy dispersive X-ray analyzer), X-ray diffraction unit (Miniflex-600) at scanning speed of 1.0 deg./min., ultraviolet -visible light spectrophotometer (Thermoscientific Evolution 300) and Keithley current-voltage characterization system. The X-ray diffraction was recorded at 40 kV with beam current of 15 mA for the sintered pellets. The diffraction angle was altered in the range of 20-70^{o}. The optical transmittance and reflectance measurements were carried out in the range of 300-1100 nm in 2 nm steps at room temperature. The transmittance was recorded through using special bands that allow hanging of the powders densely. The powders were obtained from the sintered pallets to keep consistency in measurements. The band was already stored in the reference compartment to reduce its effect. The temperature dependent conductivity measurements were performed in a homemade cryostat in ambient atmosphere in the temperature range of 300-470 K. The electrical contacts were made using high purity silver and carbon pastes. During this process, the samples were masked with four probe mask and the mask slots were smoothly pained with Ag or carbon using a brush. The C and Ag contacts were left to dry for 24 hours in isolated media. No contact annealing was made to the samples. The validity of the contact was checked by the ohmic nature of the current-voltage characteristics. The Ag contact was selected owing to its least noise in measurements.

3. Results and Discussion

In order to get sure that the samarium and yttrium doping agents is homogeneously solved in the neodymium stannate solid state solution, various regions were selected from the surfaces and from the bulk of the samples and were monitored by both of the scanning electron microscopy (SEM) and energy dispersive X-ray spectroscopy (EDX) techniques. In accordance with the recorded EDX spectra which are shown in Fig. 1 (a) and (b) for yttrium and samarium doped pyrochlore ceramics, respectively, the pyrochlore ceramics are composed of Nd, Sn , O and the doping agents only. Except for ignorable amount of carbon, no extra elements were detected in the pyrochlore. The presence of carbon is most probably due to the surface contacts on top of the samples. Point contacts of carbon were installed on the surface of the samples for the purpose of ohmic nature testing as mentioned in the experimental part. The strong Au peaks appeared as a result of 10 nm coating of the samples to prevent electron contamination. The numerical investigations on various regions of the samples revealed an average value of 4.29 at.% of yttrium and 3.49 at. % of samarium. The difference between the measurements of the selected areas never exceeds 10% of the measured value. The same spectra are always observed for all the measured values. The difference between the atomic contents that were substituted through experiments as 4.0 % of Sm_2O_3 and Y_2O_3 and those determined from EDX measurements for Sm and Y is ascribed to the escape of some of the content during the heating cycles and due to the erroneous distribution of some grains in the bulky samples. On the other hand, the respective electron microscopy images which are detected from the surfaces and bulk (cross-sectional parts) of the samples have shown much difference between the samples indicating the strong effect of the doping agents on the morphological properties of the pyrochlore. Particularly, while the Y-doped $Nd_2Sn_2O_7$ samples which are shown in Fig. 2 (a) displayed large irregularly shaped grains with very different sizes in the range of 100 nm-1.5 μm, the samarium doped samples which are shown in Fig. 2 (b) exhibit irregularly shaped grains of length of 320 and width of

230 nm. It is clear from Fig. 2 (a) and (b) that the doping agents play vital role in the shapes of the grown grains. Enlargements of the images by ~40000 times which are shown in the insets of Fig. 2 (a) and (b) for Y-and Sm-doped samples, respectively, have shown the existence of circular holes inside the grain of Y-doped samples. The diameter of these holes is ~160 nm. Such holes did not exist in the Sm-doped samples.

To clarify these differences in the SEM images, the X-ray diffraction technique is employed. The X-ray diffraction patterns for the undoped, Y and Sm doped neodymium stannate ceramics are displayed in Fig. 3. As seen, interesting characteristics can be detected from the observed XRD patterns. Particularly, while the Y-doped $Nd_2Sn_2O_7$ display the same reflection peaks of the undoped ceramics with some additional peaks (shown by dashed red circle in Fig. 3) that can be assigned to the cubic structure of the $Nd_2Sn_2O_7$ compound, the samarium doped samples displays different structural characteristics. The maximum reflection peaks of the undoped, Y-doped and Sm-doped samples appeared at diffraction angles (2θ) of 29.36^{o}, 29.66^{o} and 43.09^{o}, respectively. To understand, the structural modifications that are associated with the doping agents, the observed diffraction patterns were analyzed with the help of "Crystdiff" and "TREOR 92" software packages. The software carries computer simulations that reproduce the XRD data of possible reflections from particular crystalline material based on the lattice parameter, space groups, crystallite size and microstrain. To explore all possible structural phases, crystallography open database codes (COD) which are listed in Table-1 were employed. Since the material is mainly composed of Nd_2O_3 and SnO_2 which exhibit hexagonal and tetragonal structures, respectively, the possibly of decomposition of the ceramic samples upon doping was also taken into account. The results of the simulator are shown in Fig. 4 (a) and (b). To make the simulation results more realistic, the microstrain value was taken as 1.0×10^{-4} and the crystallite size was assumed to be 100 nm which is the worst possible size observed in the SEM analyses. As can be seen from the figure, the

theoretically and experimentally (Fig. 3) estimated reflection peaks of the $Nd_2Sn_2O_7$ ceramics are different from those of the Nd_2O_3 and SnO_2 indicating the successful production of the ceramics. Even though the theoretically estimated XRD patterns of the $Nd_2Sn_2O_7$ ceramics are highly oriented along the (022) direction which appears at diffraction angles of $2\theta = 23.91^o$, the experimentally observed main peak is oriented along the (222) reflection direction which appears at $2\theta = 29.36^o$. In addition, the possibility of material decomposition upon doping is excluded when the theoretically estimated reflection patterns of Y_2O_3 and Sm_2O_3 are compared to that of $Nd_2Sn_2O_7$. The experimentally determined patterns for Sm- doped neodymium stannate which give the strongest diffraction at $2\theta = 43.09^o$ does not appear in the patterns of the theoretically estimated XRD plot for Sm_2O_3, Nd_2O_3 and SnO_2 that are shown in Fig. 4 (a) and (b). The experimental diffraction patterns for the Sm doped samples appear at 2θ values of $43.09^o, 50.14^o, 59.23^o$ and 61.99^o. None of these diffraction angles refer to SnO_2 or to Nd_2O_3 indicating that new crystalline phase has appeared as a result of Sm doping. Attempts to explore the resulting new structure with the observed reflection peaks included test assuming cubic, hexagonal, trigonal and tetragonal cells. The orthorhombic, monoclinic and triclinic crystal systems were excluded as the number of observed reflection peaks is insufficient to execute such type of solutions. The results of the tested systems are illustrated in Table-2. As seen from the table, the most appropriate solutions which exhibit no error ($\Delta\theta$) between the experimentally observed and theoretically calculated 2θ values relate to both hexagonal and trigonal lattices with the same lattice parameters. The main difference between these two crystal systems are the number of fold axes. The hexagonal system is composed of four axes, three of equal lengths, separated by equal angles and lie in the same plane, the fourth axis is perpendicular to the plane of the other three axes. This system has lattice point in each of the two six folded axes. On the other hand, the trigonal system is composed of three equal axes, but none of them is perpendicular to the other. The crystal faces of trigonal system all have the same shape and length. These

basic definitions of the hexagonal and trigonal systems explain the reason beyond reading the same Miller indices (hkl) for the observed reflection planes and calculating the same lattice parameters for both systems.

To give significance for the observed remarkable structural changes upon doping of the neodymium stannate with Sm compared to the yttrium which reveal lattice constants of value of a =10.429 Å and also compared to the previously reported gadolinium (a =11.565 Å) and terbium (a =11.544 Å) [8] doping agents, we track the attention to the crystal structure, electronic structure, coordination number and ionic radiuses of the cations at the A and B sites of the ($A_2B_2O_7$) pyrochlore ceramics. In general, in pyrochlore oxides, $A_2B_2O_7$ is derived from fluorite by removing one eighth of the oxygen ions and ordering the two cations and oxygen anions. The $Nd_2Sn_2O_7$ structure is formed if the cation radius of the two cations (Nd, Sn) falls into a specific range. The Nd and Sn cations are of 8 and 6 coordination numbers, respectively. The ionic radius of Nd (112 pm [11]) is larger than that for Sn (69 pm [11]). The formation of $Nd_2Sn_2O_7$ basically depends on the ionic radius of the cations. For cations (A^{+3}, B^{+4}), the condition on the ionic radius must be such that: $1.46 < \frac{r_A}{r_B} < 1.80$ while for cations (A^{+2}, B^{+5}), the condition on the ionic radius must be such that: $1.40 < \frac{r_A}{r_B} < 2.20$ [12].

Recalling that the ionic radiuses of Y^{+3} and Sm^{+3} and the cations ratios (r_A/r_B) are 102 and 109 pm and 1.48 and 1.62 [11], respectively all the doping agents should form stable doped pyrochlore. In addition, a deep look at the bond length of the coordinated atoms shows that the Nd-O form a bond of length of 2.47 Å [8], the Y-O [13] and Sm-O form bonds of length of 2.30 and 2.36 Å [14], respectively. The doping of Y and Sm metals as substitutional elements in place of Nd reveals bond length differences of 0.17 and 0.11 Å, respectively. Studies on Y_2O_3 films have shown that a lower coordination number and shorter bond lengths may be achieved upon loss of oxygen atoms [15]. The absence of oxygen atoms leads to the formation of vacancies that increases the defects in the pyrochlore and causes lattice

distortion as a result of local strain fields. Vacancies cause a decrease in the interatomic distances which is accompanied to an increase in the disorder [15]. For the purpose of obtaining specific information about the defect density in the doped $Nd_2Sn_2O_7$ pyrochlore ceramics, the maximum peak broadening (β) and the diffraction angle (2θ) were used to determine the crystallite size (one grain is accumulation of many crystallites) using Scherrer equation ($D = \frac{0.94\lambda}{\beta\cos(\theta)}, \lambda = 1.5405$ Å), the microstrain ($\varepsilon = \beta/(4\tan(\theta))$ and the defect density ($\delta = 15\varepsilon/(aD)$) [4]. While the Y-doped ceramics exhibit, D, ε and δ values of 25 nm, 5.6×10^{-3} and $3.19 \times 10^{11}\ lines/cm^2$, respectively, the Sm doped samples reveals respective values of 33 nm, 2.98×10^{-3} and $1.24 \times 10^{11}\ lines/cm^2$. As the data predicts, the Y doping leads to large values of defect density compared to that of Sm. Remarkable decrease in the defect density and in the microstrain values are also obtained for Sm doped ceramics. In addition, the decrease in the lattice parameter of the pure $Nd_2Sn_2O_7$ from 10.573 to 10.429 Å upon Y doping can be assigned to the shorter bond length of Y-O compared to Nd-O as we mention here. Studies on the structural stabilization of Y- doped zirconia [16] has shown that the Y atoms occupy the second-nearest-neighbor cation sites to oxygen vacancies and repel each other. The Y atoms force oxygen vacancies to form repulsive pairs. These effective defect pairs caused phase transformation from tetragonal to cubic transition and strongly alters the lattice parameters. For our case, the preferred phase transitions in the presence of Sm are still a challenge and need further considerations.

It is possible to think that, the orbital overlapping between atoms of A site could be an extra parameter that leads to the phase transition in the presence of Sm. While Y exhibits electronic configuration of $4d^1\ 5s^2$, the Sm has the $4f^6\ 6s^2$ electronic configuration. Sm atom orbitals reach higher energy levels of Nd ($4f^4\ 6s^2$) than that of Y. It means that the orbital overlapping between Nd and Sm atoms is much stronger than that of Y and Nd. As weak overlapping (weak bonding) between orbitals leads to a very reactive surface and resulting in a more energetically stable semiconducting surface upon the adsorption of

foreign chemical species [17], the strong orbital overlapping forces formation of strong bonds and nonreactive surfaces. For this reason, we believe that, under these conditions, the internal energy (caused by strain field) stabilization could be reached by structural transformations as we observed for Sm doped $Nd_2Sn_2O_7$. As a supportive information, it is mentioned that in MoS_2/silicene and MoS_2/stanene sandwich structures [18], owing to the orbital overlapping at the interface, low biaxial deformation (~3%) was sufficient to induce the structural phase transition in MoS_2 lattice. The origin of such behavior was assigned to the strain induced interlayer covalent bonds formation, which forces MoS_2 lattice to be more sensitive to external strain. As an alternative impressive effect of the Sm doping in ceramics, it is mentioned that Sm doping caused phase evolution in $Bi_{1-x}Sm_xFeO_3$ solid state solutions. In these types of ceramics, it was observed that upon calcination, Sm doping of bismuth ferrite promotes the formation of perovskitic phase and leads to the elimination of the secondary phases [19].

To obtain information about the effects of Y and Sm doping on the optical and electrical properties of the $Nd_2Sn_2O_7$ pyrochlore ceramics, the optical absorption (A) and electrical conductivity (σ) were measured as functions of incident light energy and temperature, respectively. The absorption spectra for the samples under study are illustrated in Fig. 5 (a). The spectra display three regions of absorption named first absorption regions in the range of 5.7-5.1 eV, second absorption regions in the range of 5.1-2.3 eV for Y-doped samples and 5.1-2.8 eV for Sm-doped samples and third absorption region in the remaining ranges of incident photon energy. While the first region is assigned to the direct allowed transitions energy band gap (E_g) as demonstrated in the inset of Fig. 5 (a) which show the Tauc's equation ($(\alpha E)^2 \propto (E - E_g), \alpha = A/d,\ d$: thickness) like trend of variation, the second and third regions refer to the absorption by interbands [8]. The same style of absorption spectra were previously observed for Gd and Tb doped $Nd_2Sn_2O_7$ pyrochlore ceramics. For Tb doped samples, the values and the variation of A with incident wavelengths was faster than that of Gd. For the Sm doped samples the absorption level is higher

than that for Y above 1.91 eV. Both doped samples show, approximately, the same slopes and values in the energy range of 1.91-1.14 eV. In this region were the interbands are dominant, the width of the interbands (E_o) which is calculated in accordance with the previously described method [8] reveals values of 1.05 and 1.10 eV for Y and Sm doped samples, respectively. These values are lower than those reported as 1.39 eV and as 1.43 eV for pure and Gd doped neodymium stannate pyrochlore ceramics respectively. The E_o values for Sm and Y doped samples are also a bit higher than those we previously determined as 0.98 eV for Tb-doped ceramics [8]. In addition, as the inset of Fig. 5 (a) shows, the energy band gap of Y-doped ceramics exhibit value of 3.0 eV. Those samples doped with Sm display energy band gap of 1.40 eV. This value of the energy band gap is confusing as it is very close to the values of the interbands width and bring to the mind the possibility of domination of the interbands owing to the strong orbital overlapping between Nd and Sm atoms as we observed from the XRD analyses. In general, the value of the energy band gap for the pure neodymium stannate is 3.40 eV [4, 8]. Literature data also reported values in the range of 3.5-4.5 eV [20]. For this reason, it can be concluded that the Y-doping reduces the energy band gap of the neodymium stannate similar to that of Gd and Tb doping agents.

Although our previous investigations have shown that the f orbital electronic contributions from Tb and Gd could be the main reason for the observed narrowing in the band gap which also apply to Sm as it has f orbitals in its structure, other reasons should also be considered to explain the narrowing of the band gap as a result of Sm and Y doping. The Sm doping abruptly decreased the energy band gap of the neodymium stannate. We believe that this remarkable decrease in the value of the energy band gap is attributable to the structural modifications that raised upon Sm doping. While the Sm changed the structure from cubic to hexagonal or trigonal and significantly decreased the lattice constant along the $c-$ axis from 10.573 [4] to 9.09 Å. The Y^{+3} doping decreased the lattice constant from 10.573 to 10.429 Å. Structural modifications which happened as a result of Sm^{+3} doping are also assigned as a

reason for the shrinkage in the value of the energy band gap of sodium borosilicate [21]. In addition, it is mentioned that the decrease in the lattice parameters in SnTe is a reason for the decrease in the value of the energy band gap [22].

On the other hand, the hot probe technique and current-voltage characteristics tests has shown that while the Sm doping causes *n*-type conduction with room temperature conductivity values of 7.29× $10^{-10}\,(\Omega cm)^{-1}$, the Y-doping resulted in $p-$type conductivity and increased the room temperature conductivity values to $11.70\times 10^{-10}\,(\Omega cm)^{-1}$. Compared to the undoped samples which exhibit n- type electrical conductivity of value of value of $1.60\times 10^{-11}\,(\Omega cm)^{-1}$ [4, 8], the Sm and Y doping increases the conductivity by ~46 and 73 times, respectively. Even though the electrical conductivity is enhanced significantly, it is still very high and set the neodymium stannate in the insulating group of materials. The temperature dependent electrical conductivity which is illustrated in Fig. 5 (b) for both samples is observed to follow the Arrhenius style of variation in which the electrical conductivity is given by the relation, $\sigma(T) \propto \exp(E_\sigma/kT)$. While the electrical conductivity appears to be active in the temperature range of 370-470 K for Y doped samples with an activation energy (E_σ) of 0.28 eV, the Sm doped samples is more active in the range of 400-470 K with E_σ value of 0.55 eV. These values are less than half of the energy band gap and indicates the formation of deep donors and deep acceptors levels below the conduction and above the valence band of the Sm and Y doped $Nd_2Sn_2O_7$ ceramics, respectively. The activation energy value being 0.55 eV obtained for n-type Sm doped ceramics is less than that we observed as 1.06 eV for $n-$type undoped ceramics and larger than those obtained as 0.48 eV for Tb doped $Nd_2Sn_2O_7$ ceramics [4, 8] indicating that new impurity levels has formed in the band gap of the material under investigations. The value of the activation energy being 0.28 eV is also larger than we obtained as 0.086 eV for $p-$ type Gd-doped [8] neodymium stannate ceramics giving evidence that the accepter levels formed by Y-doping are deeper than those formed by Gd-doping. The change in the

conductivity upon doping was also observed for ZnO and was assigned to the cation vacancies and to the different incorporation of compensating donor defects [23]. The *p*-type conduction in ZnO requires incorporation of shallow acceptor levels which was achievable by substitution of a group I elements presented by potassium in Zn sites motivating the formation of one hole per alkali atoms in the neighboring oxygen atom. It is also observed that in NiO_x the conductivity type changes from *p* to n-type owing to the scenario in which for every removed O_2 ion, there is a Ni^{+2} ion taking two electrons and converting to the Ni^0 state [24, 25].

4. Conclusions

In this study, we have explored the effect of yttrium and Sm doping agents on the structural, optical and electrical properties of neodymium stannate pyrochlore ceramics which are prepared by the solid state reaction technique. Remarkable changes presented by structural modification from cubic to hexagonal (or trigonal) structural type accompanied with large shrinkage in the energy band gap and enhancement of electrical conductivity by 46 times and formation of deep donor levels at 0.55 eV are obtained via 3.49 at. % Sm doping. An atomic content of 4.29 at. % successfully changed conductivity type of the pyrochlore and increased the electrical conductivity by 73 times without much reduction in the value of the energy band gap and without changing structure of the pyrochlore. While the Sm doping nominate the neodymium stannate as an optoelectronic material being effective in the infrared range of light, the yttrium doping make the pyrochlore sensitive to visible light especially in the blue light range.

Acknowledgments

The authors would like to thank the Scientific Research Council of the Arab American University (AAUJ) of Palestine and the Scientific and Technological Research Council of Turkey (TU BITAK)

for the financial support. The work was supported by the TUBITAK under the Project FEN-E-120613-0266 and by the AAUJ under the Project Code (2018-2019 Cycle I).

References

[1] Jamil A, Schläfer J, Gönüllü Y, Lepcha A and Mathur S 2016 *Crystal Growth & Design* 16 5260-5267.

[2] Morassaei M S, Zinatloo-Ajabshir S and Salavati-Niasari M 2017 *Advanced Powder Technology* 28 697-705.

[3] de Réotier P.D, Yaouanc A, Maisuradze A, Bertin A, Baker P.J, Hillier A D and Forget A 2017 *Physical Review B* 95 134420.

[4] A A Saleh, Qasrawi A F, Yumuşak G, Mergen A 2017 *Mater. Sci-Poland* 35 534-538.

[5] Ma, C., Zhou, W., Gan, Z., Wang, X., Tan, W., Zhang, Z. and Zhai, Z., 2019. Upconversion photoluminescence modulation by electric field poling in Er3+ doped (Ba0. 85Ca0. 15)(Zr0. 1Ti0. 9) O3 piezoelectric ceramics. *Journal of Alloys and Compounds*, *794*, pp.325-332.

[6] Gokul Raja, T.S., Dheebikha, K., Balamurugan, S., Palanisami, N. and Reshma, A., 2020. Enhanced Band Gap, Optical and Near-Infra-Red Reflecting Properties of Environmentally Benign Synthesized Nanocrystalline Gd2Ti2O7 Pyrochlore Materials. *Journal of nanoscience and nanotechnology*, *20*(4), pp.2277-2285.

[7] Liu X, Wang Z, AI L, Zhu H, Wang L, Ma Z and Zhang Z 2016 *Nanoscience and Nanotechnology Letters* 8 1007-1013.

[8] Saleh A A , Hamamera H Z, Khanfar H K, Qasrawi A F, and Yumusak G 2018 *Mat. Sci. Semicon. Proc.* 88 256-261.

[9] Kim, M., Ju, H. and Kim, J., 2019. Single crystalline Bi2Ru2O7 pyrochlore oxide nanoparticles as efficient bifunctional oxygen electrocatalyst for hybrid Na-air batteries. *Chemical Engineering Journal*, *358*, pp.11-19.

[10] Ai, L., Wang, Z., Gao, Y., Cui, C., Wang, B., Liu, W. and Wang, L., 2019. Effect of surface and bulk palladium doping on the catalytic activity of La 2 Sn 2 O 7 pyrochlore oxides for diesel soot oxidation. *Journal of materials science*, *54*(6), pp.4495-4510.

[11] Martienssen W and Warlimont H. eds 2006 *Springer handbook of condensed matter and materials data* Springer Science & Business Media.

[12] Jiang S P and Shen P K eds 2013 *Nanostructured and advanced materials for fuel cells* CRC Press.

[13] Ostanin S, Craven A.J, McComb D.W, Vlachos D, Alavi A, Paxton A.T. and Finnis M.W 2002 *Physical Review B* 65 224109.

[14] Hasan N and Iftikhar K 2019 *New Journal of Chemistry* 43 4391-4405.

[15] Xue-Rui C, Hai-Yang D, Ze-Ming Q, Yu-Yin W and Guo-Bin Z 2013 *Chinese Physics C* 37 098002.

[16] Ding H, Virkar A V and Liu F 2012 *Solid State Ionics* 215 16-23.

[17] Houssa M, Pourtois G, Heyns M M, Afanas'ev V.V. and Stesmans A 2011 *Journal of The Electrochemical Society* 158 H107-H110.

[18] Ouyang B, Xiong S, Yang Z, Jing Y and Wang Y 2017 *Nanoscale* 9 8126-8132.

[19] Nalwa K S and Garg A 2008 *Journal of Applied Physics* 103 044101.

[20] Alemi A. and Ebrahimi Kalan R 2008 *Radiation Effects & Defects in Solids* 163 229-236.

[21]Munishwar S S R, Roy K and Gedam R S 2017 *Materials Research Express* 4 105201.

[22] Hsieh T H, Lin H, Liu J, Duan W, Bansil A and Fu L, 2012 *Nature communications* 3 982.

[23] Gupta, M K, Sinha N, Singh B K and Kumar B, 2010 *Materials Letters* 64 1825-1828.

[24] Molaei R, Bayati M R, Alipour H M, Nori S and Narayan J, 2013 *Journal of Applied Physics* 113 233708.

[25] Itapu S, Georgiev D G, Uprety P and Podraza N J, 2017 *physica status solidi (a)* 214 1600414.

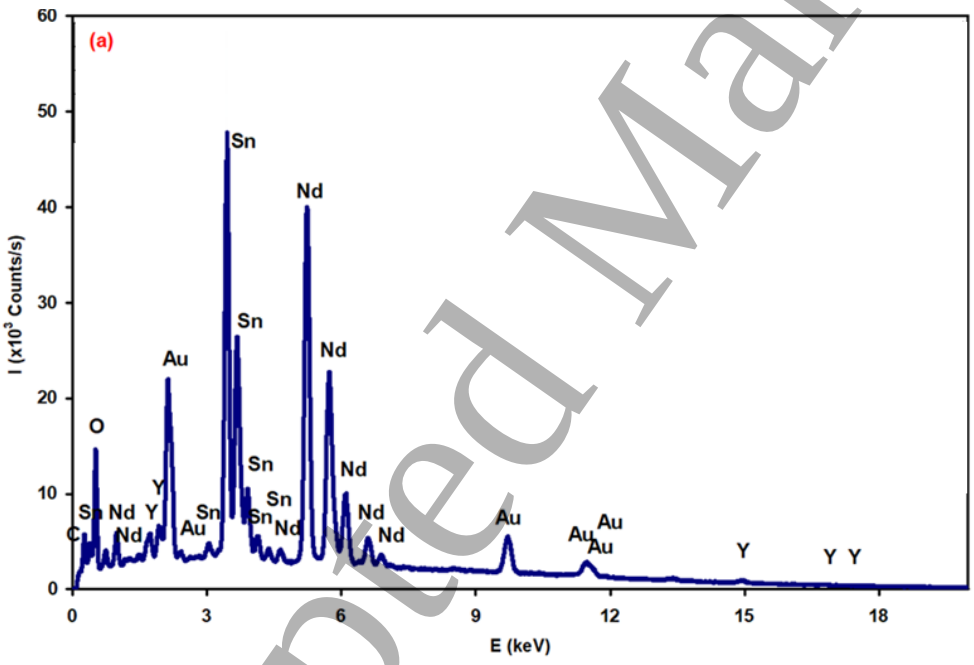

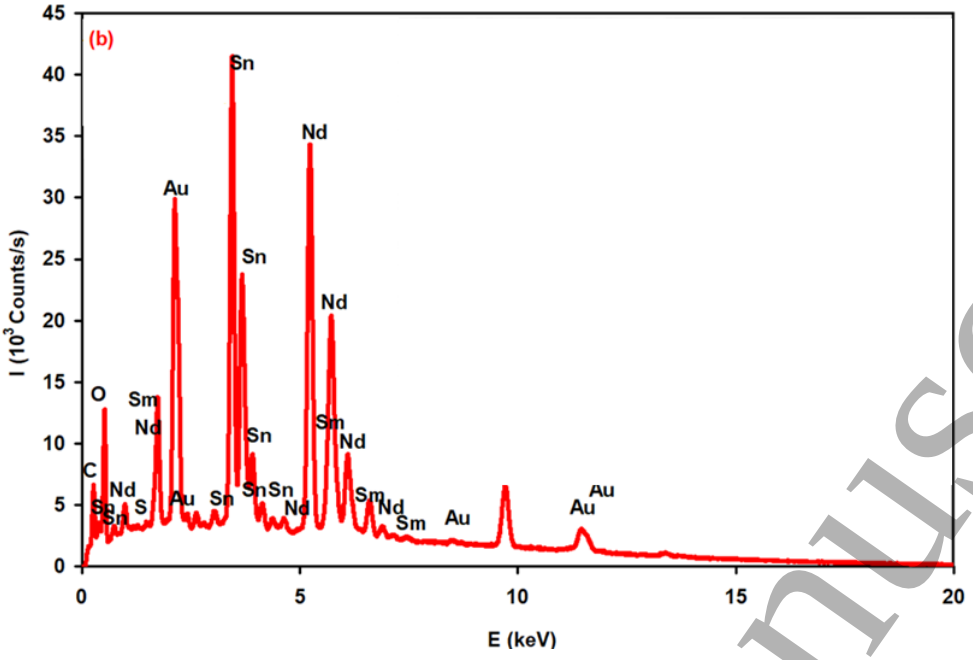

Fig. 1 The energy dispersive X-ray spectra for the (a) Y –doped and (b) Sm-doped $Nd_2Sn_2O_7$ ceramics.

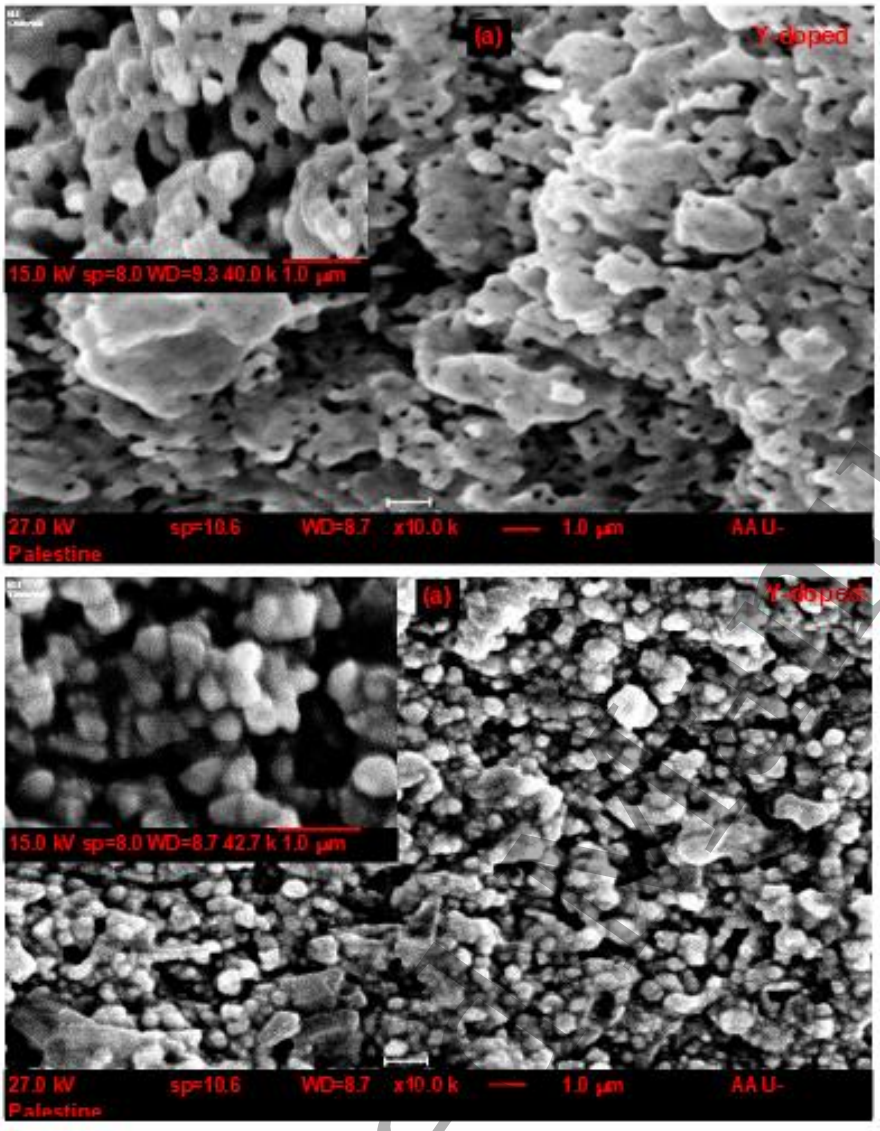

Fig. 2 the scanning electron microscopy images for (a) the Y- and (b) Sm-doped $Nd_2Sn_2O_7$ samples, respectively. The inset of (a) show the magnification at 40000 times for the Y-doped samples and inset of (b) show the magnification of 42700 times for the Sm-doped samples.

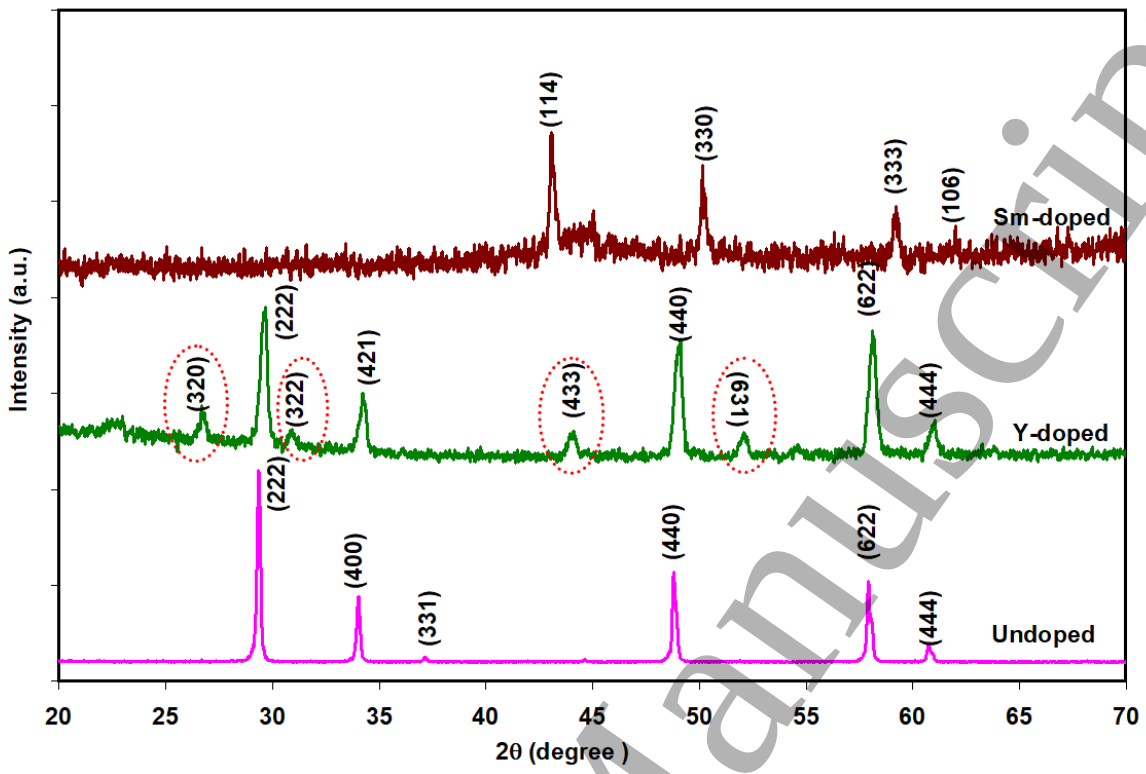

Fig. 3 The X-ray diffraction patterns for $Nd_2Sn_2O_7$ pyrochlore ceramic doped with Y and Sm.

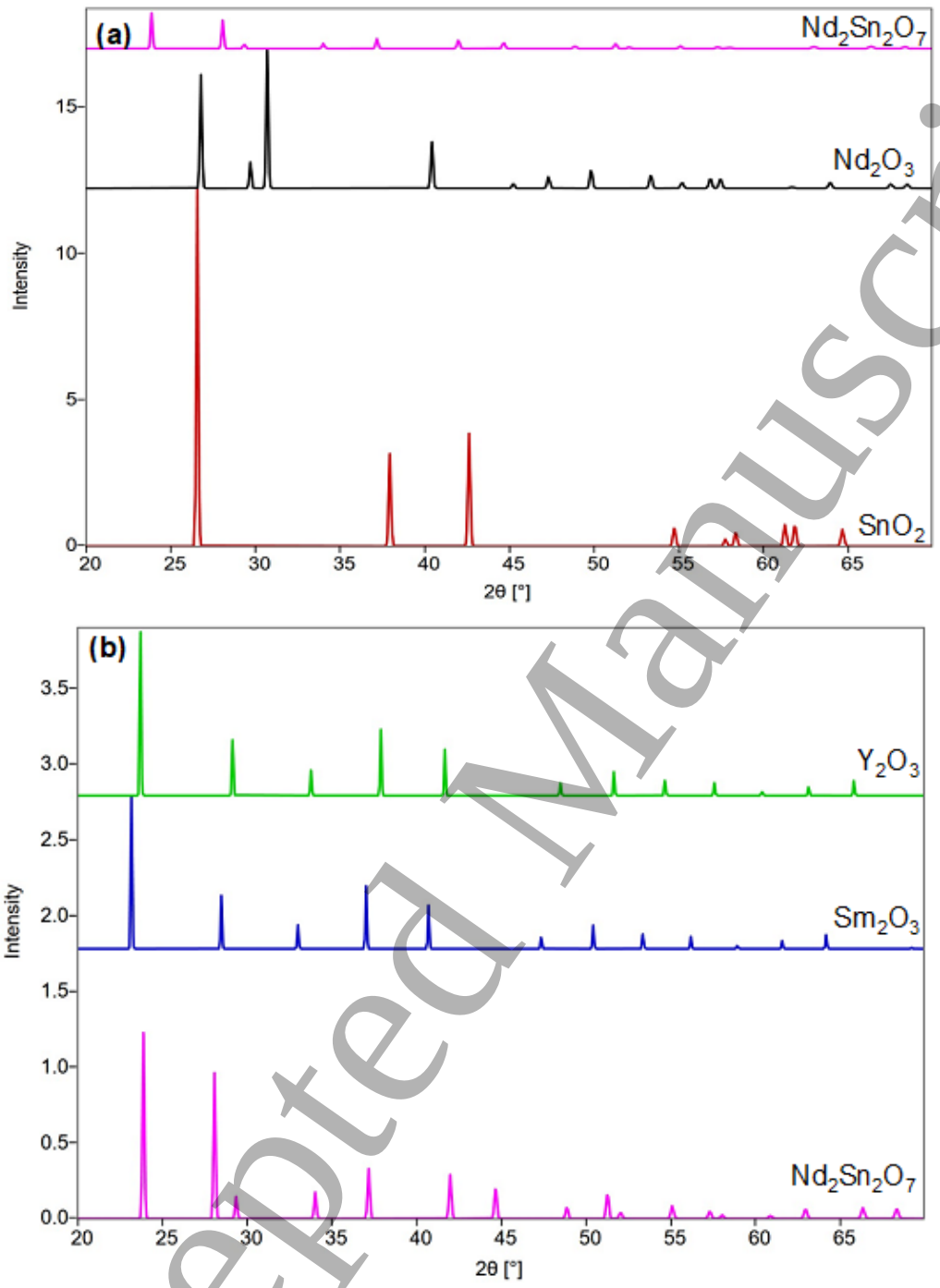

Fig. 4 The simulated X-ray diffraction patterns for (a) $Nd_2Sn_2O_7$, Nd_2O_3 and SnO_2 and for (b) $Nd_2Sn_2O_7$, Y_2O_3 and Sm_2O_3.

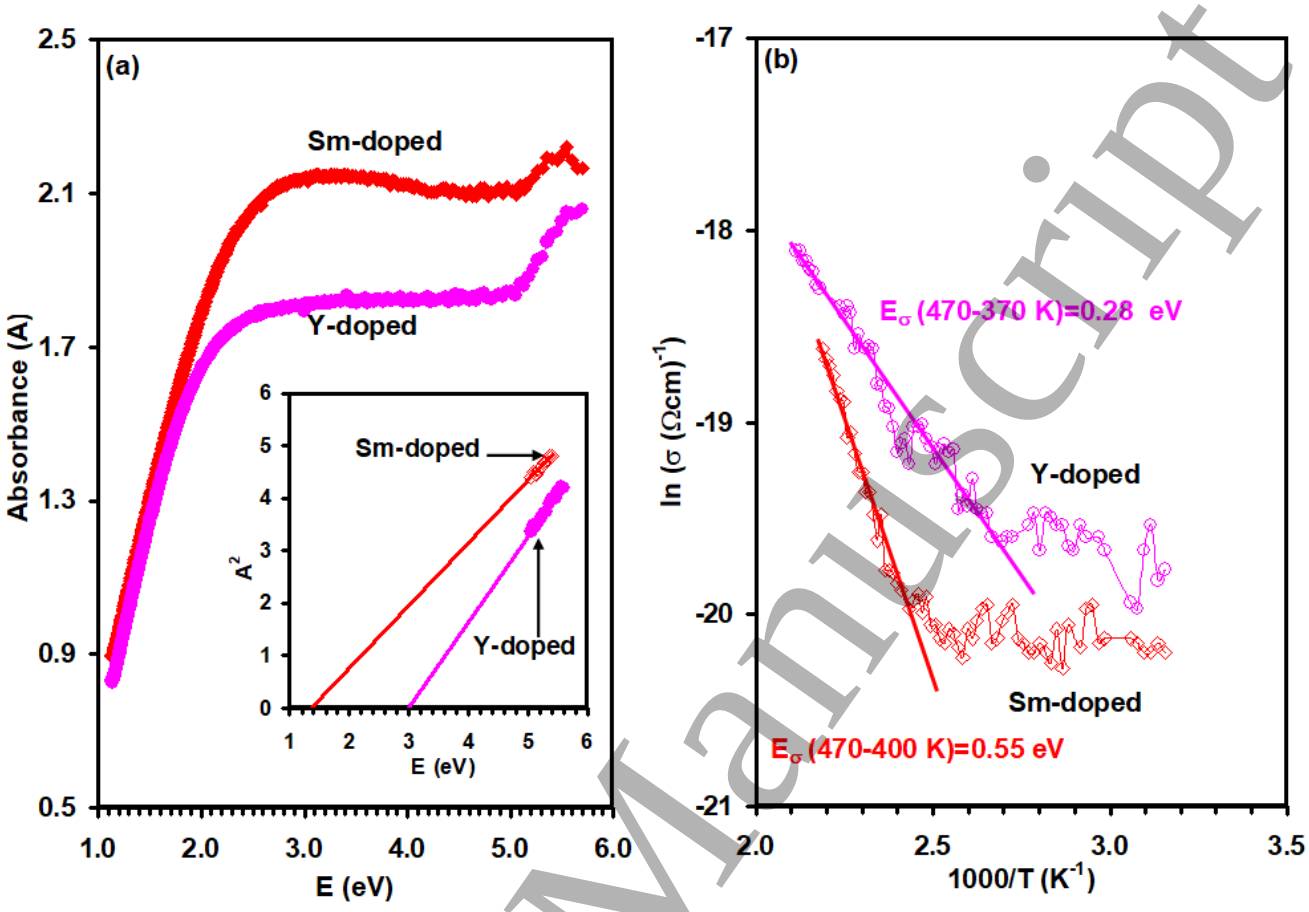

Fig. 5 (a) the optical absorbance and Tauc equation like fittings (inset of figure) for the Y- and Sm-doped $Nd_2Sn_2O_7$ pyrochlore ceramics. (b) The temperature dependent electrical conductivity for the Y and Sm-doped $Nd_2Sn_2O_7$ pyrochlore ceramics.

Table 1: The structural parameters of the compounds composing the Sm and Y doped $Nd_2Sn_2O_7$ ceramics

COD	Chemical Formula	Space Group	Lattice parameters			Crystal Structure
			a (Å)	b(Å)	c(Å)	
1009013	Y_2O_3	I a -3	10.61	10.61	10.61	Cubic
1000062	SnO_2	P 42/m n m	4.74	4.74	3.19	Tetragonal
1010281	Nd_2O_3	P 3 2 1	3.84	3.84	6.01	Hexagonal
1010340	Sm_2O_3	I 21 3	10.85	10.85	10.85	Cubic

Table -2: The possible crystal systems that results from the Sm doping into the structure of $NdSn_2O_7$

Observed		Cubic $a = 8.89$ Å		Hexagonal $a = 10.91$ Å $c = 9.09$ Å		Trigonal $a = 10.91$ Å $c = 9.09$ Å		Tetragonal $a = 14.11$ Å $c = 2.12$ Å	
$2\theta\ (^o)$	I/I_o	$2\theta\ (^o)$	$\Delta\theta(^o)$	$2\theta\ (^o)$	$\Delta\theta(^o)$	$2\theta\ (^o)$	$\Delta\theta(^o)$	$2\theta\ (^o)$	$\Delta\theta(^o)$
43.09	100	43.09	0.00	43.09	0.00	43.09	0.00	43.09	0.00
50.14	78	50.18	0.04	50.14	0.00	50.14	0.00	50.14	0.00
59.23	56	59.63	0.40	59.23	0.00	59.23	0.00	59.24	0.01
61.99	43	61.61	0.38	61.99	0.00	61.99	0.00	61.98	0.01